Polarization dependence of optical absorption and emission in quantum wires

Peter C. Sercel and Kerry J. Vahala
Department of Applied Physics, Mail Stop 128-95, California Institute of Technology, Pasadena, California 91125
(Received 19 October 1990; revised manuscript received 17 January 1991)

The polarization dependence of absorption and emission spectra in cylindrical quantum wires is studied using a formulation of multiband envelope-function theory in a representation of cylindrical Bloch waves. The work presented is an analysis of the optical properties of quantum wires, which includes band-coupling effects. Contrary to the assumptions employed in previous studies, the valence states involved in these transitions are a strong admixture of light- and heavy-hole character. Band-coupling effects are therefore essential to understanding valence-subband dispersion and density of states, the energy dependence of interband optical-transition matrix elements, and polarization anisotropies. Analytical expressions are derived for the polarization dependence of optical matrix elements, and hence, optical-absorption and emission spectra. Applicability of the results derived for cylindrical quantum wires to the case of wires with lower symmetry is discussed.

I. INTRODUCTION

Research on quantum-wire and quantum-dot nanostructures, the reduced dimensional analogs of the conventional planar quantum well, has been motivated largely by the promise these structures hold for improved optoelectronic device applications.[1-3] In particular, the feasibility of incorporating quantum wires into the active region of a semiconductor laser has recently been experimentally demonstrated.[4] In light of this achievement, the question of how to optimally configure a quantum-wire laser becomes technologically important. More precisely, the question may be stated, what relative orientation between a quantum wire and an optical field will produce maximum interaction? Although previous studies have addressed this question using one-band effective-mass theory,[5-8] recent theoretical work by the authors has clearly demonstrated that one-band theory is inappropriate to the study of valence-band states in quantum wires and that band-coupling effects are critical to a correct analysis of this problem.[9-12] In this work, we present an account of a detailed study employing a coupled-band technique[9-12] to calculate the valence-subband dispersion relations, density of states (DOS), interband optical-transition matrix elements, and absorption and emission spectra of cylindrical quantum wires of various radii. In addition to providing a theoretical framework with which to interpret polarization-dependent absorption-emission spectra of quantum wires, these calculations can aid in the design of quantum-wire lasers. As an example, Figs. 1(a) and 1(b) represent lasers in which the quantum wires are oriented parallel and perpendicular to the cavity axis, respectively.

Recent experimental studies suggest that these two configurations should be inequivalent. Utilizing polarization-dependent photoluminescence excitation (PLE) spectroscopy, a strong relative anisotropy between the two lowest-energy optical transitions in quantum-wire arrays has been observed.[7,8,13] These results have been interpreted in the context of a one-band model, in which the two transitions are identified as conduction-to-heavy-hole and conduction-to-light-hole exciton lines, under the assumption that the valence states are decoupled at the zone center of the quantum wire. As mentioned above, this assumption represents a serious shortcoming—in

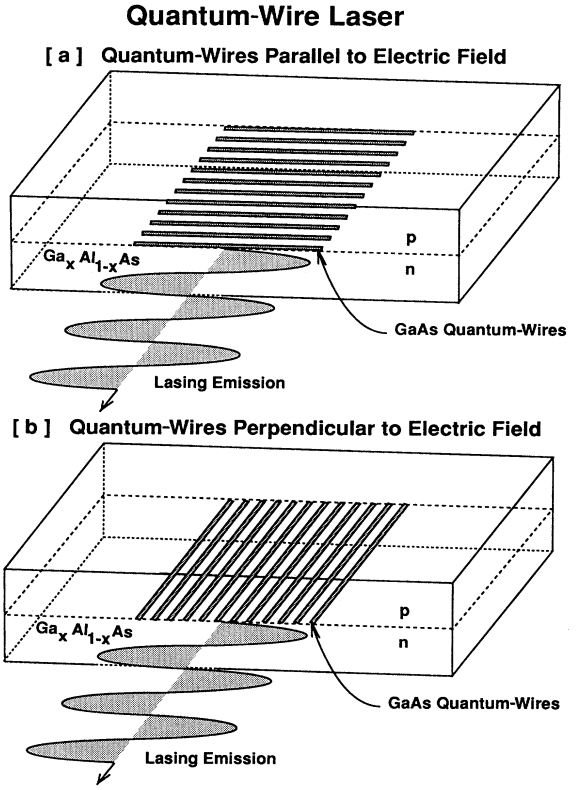

FIG. 1. Two possible schemes for a quantum-wire laser. (a) Quantum wires oriented parallel to the cavity facets; (b) quantum wires oriented parallel to the cavity axis. In both structures the quantum wires are situated inside a graded index region and the laser is assumed to operate in TE mode.

Refs. 9–12, the present authors have demonstrated that the light- and heavy-hole valence bands are strongly coupled in these structures, even at the zone center. The reported agreement of the one-band theory with the PLE measurements in Refs. 7 and 8 is in fact a consequence of a second unjustified assumption that coherence terms may be neglected in the calculation of the optical-transition matrix element.[12] When these coherence terms are restored, the one-band model predicts no relative anisotropy.[12] The observed polarization dependence, however, is explained by the coupled-band approach of Ref. 12, which forms the basis of this work.

The successful explanation of the *relative* anisotropy observed in Refs. 7, 8, and 13 requires only calculation of optical-transition matrix elements at the zone center.[12] However, the theoretical comparison undertaken in this work of the *absolute* strengths of various transitions as a function of field orientation and wire size also requires knowledge of the energy dependence of the transition matrix element and the joint density of states (JDOS) for optical transitions. The structure of the dispersion relations for certain subbands will be seen to be electronlike, resulting in a large JDOS for transitions involving these subbands, a fact that has important consequences to the optical-absorption and emission spectra in these structures. In Sec. II we begin with a brief review of the formalism necessary to calculate these quantities.

II. ELECTRONIC STRUCTURE OF THE CYLINDRICAL QUANTUM WIRE

The determination of optical-transition matrix elements and DOS for the quantum wire involves several distinct steps. First, it is necessary to determine the conduction-subband dispersion relations and wave functions. This step may be accomplished by invoking a simple one-band effective-mass theory, in which the quantum wire is modeled as a two-dimensional potential well, in analogy with calculations that have been performed on the conventional one-dimensional quantum well.[2] Second, the more complicated, coupled valence-band problem must be solved to yield valence-subband wave functions and dispersion relations. Once these steps are carried out, it is then straightforward to calculate matrix elements and JDOS for interband optical transitions. The calculations that follow assume a cylindrical quantum wire with a finite well depth. The high symmetry permits us to describe the polarization dependence of optical transitions with simple trigonometric expressions, which will be derived in an intuitive way, yet the analysis retains the essential physics of the problem: namely, two-dimensional quantum confinement with finite well depths in a coupled-band system. We will show in Sec. III C, however, they many of the qualitative features of the analysis for cylindrical wires should be reproduced in the lower symmetry structures (quantum wires of a square, rectangular, and triangular cross section).

A. Conduction subbands

The conduction-subband wave functions and energies in the cylindrical quantum wire may be calculated straightforwardly with the one-band effective-mass theory.[2] The conduction wave function takes the form

$$\Psi^{C}_{L_z,\pm 1/2}(k_z)=\frac{1}{N_c}\begin{bmatrix} J_{L_z}(k_{L_z,n}r)(r<R) \\ H_{L_z}\left(\sqrt{k^2_{L_z,n}-\frac{2m_c^* V_c}{\hbar^2}}\,(r>R)\right)\end{bmatrix} \times \exp(iL_z\theta)\exp(ik_z z)\left|\tfrac{1}{2},\pm\tfrac{1}{2}\right\rangle , \quad (1)$$

where J and H are Bessel functions and Hankel functions, and the radial wave number $k_{L_z,n}$ is a discrete quantity determined by the requirement of continuity of the envelope and its derivative across the interface between the well and barrier regions. The radius of the wire is R and the conduction-band offset is V_c. The energy of the state is given by $E_c(k_z)=\hbar^2/2m_c^*(k^2_{L_z,n}+k_z^2)$. For simplicity m_c^* is taken to be the same inside and outside the wire. N_c is a coefficient that normalizes the wave function. The term $|\frac{1}{2},\pm\frac{1}{2}\rangle$ is simply the conduction-band Bloch function with spin up or down. In what follows we will adopt the convention whereby the conduction subband that corresponds to a particular value of $|L_z|$ is labeled "$C(L_z)$." The lowest subband $C(0)$ has even parity in the plane perpendicular to the wire, and is only doubly degenerate (due to the spin degeneracy of the Bloch function). The next subband $C(1)$ has quantum number $L_z=\pm 1$ and therefore is fourfold degenerate. This state has odd parity in the plane perpendicular to the wire axis. As a matter of terminology, from this point on when we refer to parity, it will be understood to indicate parity in the plane perpendicular to the wire.

B. Valence subbands

The valence-band states of the quantum wire represent a more challenging problem than the conduction states just discussed. In the simplest approximation, the two split-off bands are assumed to be decoupled from the four Γ_8 bands (the light and heavy holes); however, even then, coupling among the remaining four bands may not be neglected so that a multiband envelope-function technique must be employed. We adopt the approach of Refs. 9–12, in which the bulk Luttinger Hamiltonian is expressed in a representation not of Bloch *plane waves,* but of the appropriate *cylindrical waves.* (The approach used here employs an explicit representation of the Hamiltonian but is equivalent to the coordinate-free approach of Ref. 14.) This basis is simply the set of eigenstates of the projection of total angular momentum along the z axis. The total angular momentum operator is the sum of the angular momenta of the envelope and Bloch components of the total wave function, defined by the relation $\mathbf{F}=\mathbf{J}+\mathbf{L}$, where $\mathbf{J}$ is the angular momentum that characterizes the familiar zone-center Bloch functions $|J,J_z\rangle$ ($J=\frac{3}{2}$ for the light- and heavy-hole states), and $\mathbf{L}$ is the angular momentum of the envelope part of the wave function.[11] Obviously, then, $F_z=J_z+L_z$, so that the necessary basis may be written in the product form

$$|k_z,k,F_z;J,J_z\rangle=|J,J_z\rangle|k_z;k,L_z=F_z-J_z\rangle . \quad (2)$$

Here the envelope vector $|k_z;k,L_z\rangle$, which has angular momentum L_z about the z axis, is represented in cylindri-

cal coordinates by

$$\langle r,\theta,z|k_z;k,L_z\rangle=\frac{i^{L_z}}{2\pi}H_{L_z}(kr)e^{iL_z\theta}e^{ik_zz}\ . \tag{3}$$

In this expression, k is a radial wave number, H_{L_z} is a Hankel function of order L_z, and k_z is the component of crystal momentum along the z axis.

This process of expressing the bulk band-structure Hamiltonian in this basis involves a unitary transformation from the conventional Bloch plane-wave representation and is described in detail in Ref. 11. It is found that the Hamiltonian is block diagonal in F_z, with subblocks corresponding to a given quantum number F_z taking the identical form[11]

$$H_{F_z}^{\Gamma_8}=\begin{array}{c}\begin{matrix}|\frac{3}{2},\frac{3}{2}\rangle|F_z-\frac{3}{2}\rangle & |\frac{3}{2},\frac{1}{2}\rangle|F_z-\frac{1}{2}\rangle & |\frac{3}{2},-\frac{1}{2}\rangle|F_z+\frac{1}{2}\rangle & |\frac{3}{2},-\frac{3}{2}\rangle|F_z+\frac{3}{2}\rangle\end{matrix}\\ \begin{pmatrix} E_v+\frac{T}{2} & -iL & -M & 0\\ iL^* & E_v+\frac{T}{6}+\frac{2Q}{3} & 0 & -M\\ -M^* & 0 & E_v+\frac{T}{6}+\frac{2Q}{3} & iL\\ 0 & -M^* & -iL^* & E_v+\frac{T}{2}\end{pmatrix}\end{array}\ . \tag{4}$$

In Eq. (4), the basis vectors are written as products of a zone-center Bloch function, $|J,J_z\rangle$, and the envelope state, $|L_z\rangle$, where $L_z=F_z-J_z$. This form ensures that all the basis vectors correspond to the same quantum number F_z. In the envelope vector, k and k_z are understood and therefore omitted. The terms in the matrix are given by

$$\begin{aligned}-\frac{T}{2}&=(\gamma_1+\gamma_2)\frac{k^2}{2}+(\gamma_1-2\gamma_2)\frac{k_z^2}{2}\ ,\\ -\left[\frac{T}{6}+\frac{2Q}{3}\right]&=(\gamma_1-\gamma_2)\frac{k^2}{2}+(\gamma_1+2\gamma_2)\frac{k_z^2}{2}\ ,\\ -L&=-i2\sqrt{3}\gamma_2\frac{kk_z}{2}\ ,\\ -M&=\sqrt{3}\gamma_2\frac{k^2}{2}\ ,\end{aligned} \tag{5}$$

where the parameters γ_1 and γ_2 are the usual Luttinger parameters, and we have invoked the spherical approximation ($\gamma_2=\gamma_3$).[15,16] E_v denotes the bulk valence-band edge, which will later be taken to be a function of position in modeling the quantum-wire heterostructure.

To calculate the eigenstates and eigenenergies of the quantum wire that correspond to a given total angular momentum quantum number F_z, we model the heterostructure as in the conduction-band calculation by introducing a radial potential V_v in the barrier region equal to the valence-band discontinuity across the interface at $r=R$. Then inside and outside the quantum wire, we find the heavy- and light-hole eigenvectors for a given quantum number F_z corresponding to a given energy and down-wire momentum k_z. We then form in each region the most general possible linear combination of these bulk eigenvectors, and impose appropriate boundary conditions. To begin with, the wave function must be regular at the origin, so that the solution in the region $r<R$ must take the general form

$$\begin{aligned}\psi_{F_z}=[\,&A_1\phi_{F_z}^{\mathrm{HH1}}(r,z)+A_2\phi_{F_z}^{\mathrm{HH2}}(r,z)+A_3\phi_{F_z}^{\mathrm{LH1}}(r,z)\\ &+A_4\phi_{F_z}^{\mathrm{LH2}}(r,z)]\quad(r<R)\ ,\end{aligned} \tag{6}$$

where the $\phi_{F_z}(r,z)$ are the bulk light- and heavy-hole eigenvectors, which are regular at $r=0$, given in Ref. 11. The wave function in the region $r>R$ is

$$\begin{aligned}\psi_{F_z}=[\,&A_5\phi_{F_z}^{\mathrm{HH1}}(r,z)+A_6\phi_{F_z}^{\mathrm{HH2}}(r,z)+A_7\phi_{F_z}^{\mathrm{LH1}}(r,z)\\ &+A_8\phi_{F_z}^{\mathrm{LH2}}(r,z)]\quad(r>R)\ ,\end{aligned} \tag{7}$$

where for bound states the $\phi_{F_z}(r,z)$ are the bulk light- and heavy-hole eigenvectors, which vanish at infinity, given in Ref. 11.

By requiring continuity of the wave function (four equations) and the probability current (four more equations) across the interface between well and barrier regions at $r=R$, we obtain an 8×8 homogeneous, linear system of equations for the eight unknown mixing coefficients $A_1,\ldots,A_8$. The requirement that the determinant of coefficients vanish for a solution to exist supplies an implicit relation determining the allowed quantum-wire eigenenergies for a given F_z and k_z. As this relation appears in Ref. 11, it is not reproduced here.

In Figs. 2(a) and 2(b) we show the subband dispersion $E(k_z)$ for bound states corresponding to $F_z=\pm\frac{1}{2}$ and $F_z=\pm\frac{3}{2}$, respectively, in a GaAs/$Al_{0.3}Ga_{0.7}$As quantum wire with radius 5 nm. Band-structure parameters have been chosen to reflect $m_{\mathrm{HH}}^*=0.45m_0$ and $m_{\mathrm{LH}}^*=0.082m_0$. There are no bound valence states for the 5-nm-radius wire in the spaces $|F_z|>\frac{3}{2}$: Figs. 2(a) and 2(b) represent all bound light- and heavy-hole states for this radius. As eigenstates in a quantum wire are gen-

erally admixtures of light- and heavy-hole character [see Eqs. (6) and (7)] even at the zone-center, we denote the states in the figures according to the label $E^{\pm}_{F_z,n}$, where E_{F_z} is the irreducible representation determined by quantum number F_z, the $\pm$ refers to zone-center parity (even or odd), and the number n refers to the order of the subband in energy at the zone center for the particular quantum number F_z. For example, $E^{+}_{1/2,1}$ denotes the uppermost subband in Fig. 2(a), which has quantum number $F_z=\frac{1}{2}$, and has even parity at the zone center. The strong nonparabolicity of the subband structure is a result of the no-crossing rule for coupled states, reflecting the importance of band-coupling effects in this system. The most extreme result of this coupling is seen in Fig. 2(b), in which the highest subband, $E^{+}_{3/2,1}$, is actually electronlike at the zone center. Similar results have been obtained previously for quantum wires with a cylindrical[11,14] and rectangular[17,18] cross section.

Having determined the subband dispersion relations of the coupled valence states of the quantum wire, it is a simple matter to derive the DOS. For a one-dimensional structure, it is well known that the DOS per unit length is given by

$$D(E)=\sum_i g_i \frac{1}{\pi}\left|\frac{dk_z^i(E)}{dE}\right|, \tag{8}$$

where i runs over all subbands, $g_i=2$ is the Kramer's degeneracy of each subband, and $k_z^i(E)$ satisfies $E_i(k_z^i)=E$. In Figs. 3(a) and 3(b) we separately present the calculated DOS corresponding to the $F_z=\frac{1}{2}$ and $\frac{3}{2}$ subbands, whose dispersion relations are plotted in Figs. 2(a) and 2(b), respectively. In these figures, the DOS functions have been convoluted with a Gaussian line-shape function with a full width at half maximum (FWHM) of 0.5 meV. The dominant feature in these plots is the large peak in Fig. 3(b) corresponding to the electronlike subband denoted $E^{+}_{3/2,1}$ in Fig. 2(b). In Sec. III B we will see that this will have a pronounced effect upon the polarization content of radiative emission from a quantum wire.

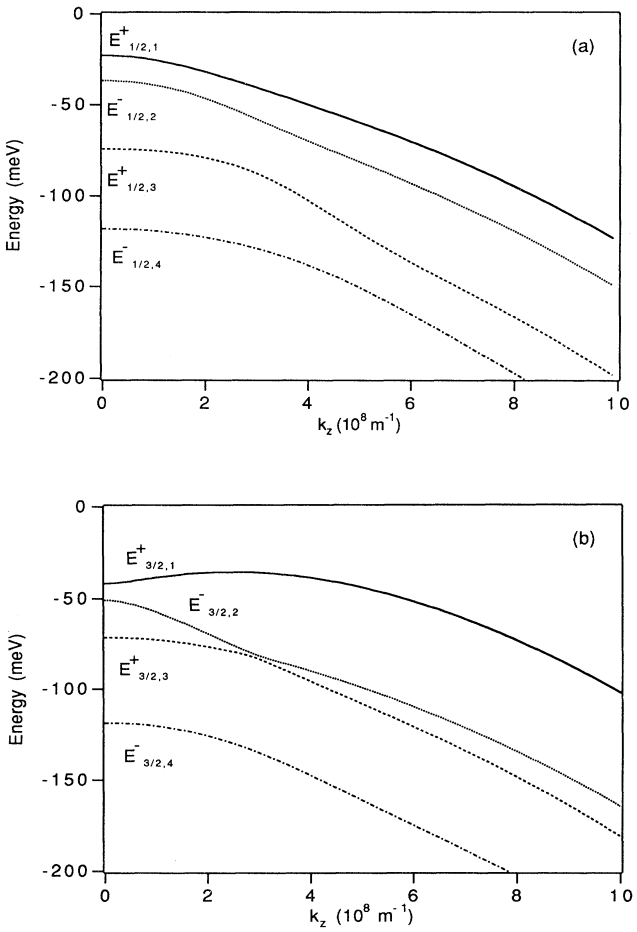

FIG. 2. Valence-subband dispersion $E(k_z)$ for a 5-nm-radius GaAs quantum wire embedded in an $Al_{0.3}Ga_{0.7}As$ barrier (well depth = 150 meV). (a) Valence subbands with quantum number $F_z=\pm\frac{1}{2}$. The dispersion curves are labeled according to the convention $E^{\pm}_{F_z,n}$, where $\pm$ denotes the parity of the zone-center state to which they correspond, and n gives the order of the subband in energy below E_v at the zone center. (b) $F_z=\pm\frac{3}{2}$. Note that the highest state in this space is electronlike near the subband edge.

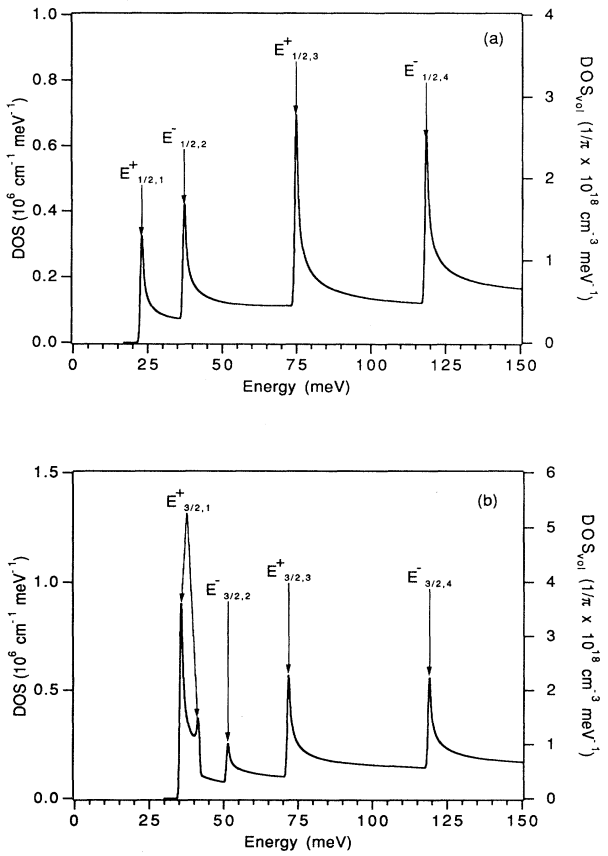

FIG. 3. DOS for a 5-nm-radius GaAs quantum wire embedded in an $Al_{0.3}Ga_{0.7}As$ barrier (well depth = 150 meV). (a) $F_z=\pm\frac{1}{2}$; (b) $F_z=\pm\frac{3}{2}$.

III. INTERBAND OPTICAL TRANSITIONS IN CYLINDRICAL QUANTUM WIRES

A. Polarization dependence of the optical matrix element

The technique outlined in the preceding section for determining the valence-subband wave functions of the quantum wire permits us to calculate the interband optical-transition matrix elements. For a given valence subband $E_{F_z,n}$ we determine the coefficients $A_1,\ldots,A_8$ in Eqs. (6) and (7) and obtain a normalized wave function of the following general form:

$$\Psi^v_{F_z,n}(k_z)=\begin{bmatrix} f^1_n(r)\exp[i(F_z-\frac{3}{2})\theta] \\ f^2_n(r)\exp[i(F_z-\frac{1}{2})\theta] \\ f^3_n(r)\exp[i(F_z+\frac{1}{2})\theta] \\ f^4_n(r)\exp[i(F_z+\frac{3}{2})\theta] \end{bmatrix}\exp(ik_z z)\ . \quad (9)$$

This vector is written in the basis of zone-center Bloch functions $|J,J_z\rangle$, taken in the order $|\frac{3}{2},\frac{3}{2}\rangle,\ldots,|\frac{3}{2},-\frac{3}{3}\rangle$. These Bloch functions are given explicitly in Ref. 11. The radial functions $f^1_n(r),\ldots,f^4_n(r)$ denote the radial components of Eqs. (6) and (7) determined for a given subband of quantum number F_z and energy index n (see Fig. 4) and are parametrically dependent on k_z. The conduction states involved in the optical transition are much simpler of course and are given explicitly in Eq. (1).

The polarization-dependent interaction of a quantum wire with an optical field may be represented by the $\mathbf{A}\cdot\mathbf{P}$ interaction Hamiltonian. Here, $\mathbf{A}$ is the polarization vector of a linearly polarized optical wave, which we take to be $\hat{\mathbf{A}}=\cos(\theta)\hat{\mathbf{z}}+\sin(\theta)\hat{\mathbf{x}}$, where z is the wire axis. Using the wave functions given in Eqs. (1) and (9) for conduction subband $C(L_z)$ and valence subband $E_{F_z,n}$, we therefore write a k_z-dependent squared transition matrix element of the general form

$$|M|^2_{C(L_z)-E_{f_z,n}}=[|\langle\psi^C_{L_z,-1/2}(k_z)|\mathbf{P}|\psi^v_{F_z,n}(k_z)\rangle\cdot\hat{\mathbf{A}}|^2+|\langle\psi^C_{L_z,1/2}(k_z)|\mathbf{P}|\psi^v_{F_z,n}(k_z)\rangle\cdot\hat{\mathbf{A}}|^2]\ . \quad (10)$$

Examination of Eqs. (1), (9), and (10) reveals two important selection rule operatives that vastly simplify our analysis. The first is that there is a k-selection rule for the z direction. The second is that there is a strict envelope angular momentum selection rule. For example, consider transitions involving the lowest conduction subband $C(0)(L_z=0)$ and any of the quantum wire valence subbands $E_{F_z,n}$ with quantum number $F_z=\frac{1}{2}$. In this case, integration over the coordinate θ eliminates all but the second component of the vector Eqn. [9]. The squared matrix element for these transitions thus simplifies to the following expression:

$$|M|^2_{C(0)-e_{1/2,n}}=(|\langle\tfrac{1}{2},\tfrac{1}{2}|\mathbf{P}|\tfrac{3}{2},\tfrac{1}{2}\rangle\cdot\mathbf{A}|^2 +|\langle\tfrac{1}{2},-\tfrac{1}{2}|\mathbf{P}|\tfrac{3}{2},\tfrac{1}{2}\cdot\mathbf{A}|^2)I^2_{0,(1/2,n)}(k_z)\ , \quad (11)$$

where all of the information about the envelopes is now contained in the radial overlap integral for the particular transition, $I^2_{0,(1/2,n)}(k_z)$. Utilizing the explicit representations for the Bloch functions, $|\frac{1}{2},\frac{1}{2}\rangle=|s\rangle\uparrow$, $|\frac{1}{2},-\frac{1}{2}\rangle=|s\rangle\downarrow$, $|\frac{3}{2},\frac{1}{2}\rangle=\sqrt{\frac{2}{3}}|z\rangle\uparrow-\sqrt{\frac{1}{6}}(|x\rangle+i|y\rangle)\downarrow$, the matrix element assumes the remarkably simple, analytical, form

$$|M|^2_{C(0)-E_{1/2,n}}=[\tfrac{2}{3}\cos^2(\theta)|P|^2 +\tfrac{1}{6}\sin^2(\theta)|P|^2]I^2_{0,(1/2,n)}(k_z)\ . \quad (12)$$

Here, P is the matrix element of the momentum operator between orbital "s" and "p" states.[19] All of the polarization dependence is contained in a simple trigonometic expression, and is the same for all transitions between the lowest conduction subband and the valence subbands with $F_z=\frac{1}{2}$. The energy dependence of the matrix element is entirely contained in the overlap integral for each transition through its dependence on k_z.

Similar simplifications apply for transitions between $C(0)$ and the valence subbands $E_{F_z,n}$ with quantum number $F_z=\frac{3}{2}$. In this case, using $|\frac{3}{2},\frac{3}{2}\rangle=-1/\sqrt{2}(|x\rangle+iy\rangle)\uparrow$, we find the result

$$|M|_{C(0)-E_{3/2,n}}=\tfrac{1}{2}\sin^2(\theta)|P|^2 I_{0,(3/2,n)}(K_z)\ , \quad (13)$$

again a remakably simple analytical form.

In Fig. 4 we show the polarization dependence of the relative squared optical-transition matrix elements for

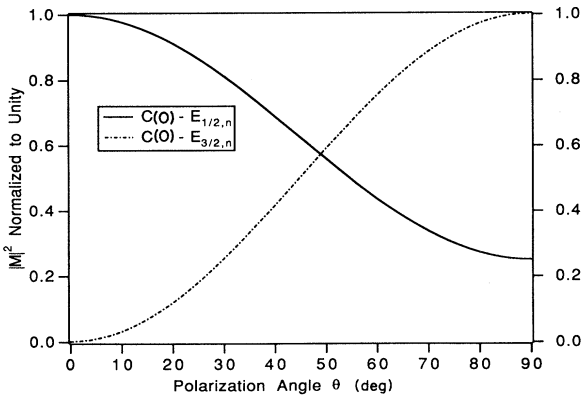

FIG. 4. Polarization dependence of the squared optical-transition matrix element for transitions between the lowest electron subband, $C(0)$, and the highest two valence subbands $E^+_{1/2,1}$ and $E^+_{3/1,1}$, respectively. The matrix elements are normalized to a maximum of unity and are plotted vs the polarization angle θ measured from the wire axis (i.e., at $\theta=0$ $\mathbf{E}$ is parallel to the wire axis). The polarization dependence is independent of the size or composition of the quantum wire.

these transitions. Note that the polarization dependence is independent of the size or composition of the quantum wire. It is clear that transitions involving the $F_z=\frac{1}{2}$ subbands are four times stronger for the electric-field vector oriented along the wire versus the perpendicular orientation. For the $F_z=\frac{3}{2}$ valence subbands, the trend is the reverse; in fact, in this model these states do not interact at all with optical waves polarized along the axis of the wire, a surprising result, but one that, as will be seen in Sec. III C, could have been anticipated on the basis of group theory. This is perhaps our most important result; the importance arises from the fact that the two lowest-energy optical transitions in the wire, respectively, are the $C(0)-E_{1/2,1}$ and $C(0)-E_{3/2,1}$ transitions. [See Fig. 2: the subband $E_{1/2,2}$ has odd parity at the zone center and hence transitions between it and $C(0)$ will be approximately forbidden on the basis of parity selection.] Figure 4 shows that these two transitions have a pronounced relative anisotropy, which will have a pronounced effect upon the polarization dependence of the absorption, emission, and hence the gain of quantum wires. This will be discussed further in Sec. III B.

In Figs. 5(a) and 5(b) we show the dependence on k_z of the overlap integrals for transitions involving $C(0)$ and each of the bound valence subbands with quantum number $F_z=\frac{1}{2}$ and $\frac{3}{2}$, Eqs. (12) and (13), respectively. These calculations were performed for a GaAs quantum wire of radius 5 nm, embedded in $Al_{0.3}Ga_{0.7}As$. Obviously, in contrast to the polarization dependence (Fig. 4), the magnitude and energy dependence of the matrix elements depend on the size and comparison of the wire. Note that at zone-center ($k_z=0$) transitions to the odd-parity valence states are forbidden. However, it is clear from the figures that the matrix elements are highly energy dependent, and that parity selection is increasingly violated as we move away from the zone center. This is a result of band coupling: As k_z increases from zero, the subbands are increasingly mixed so that subbands with odd parity at the zone center pick up an increasing degree of even-parity character.

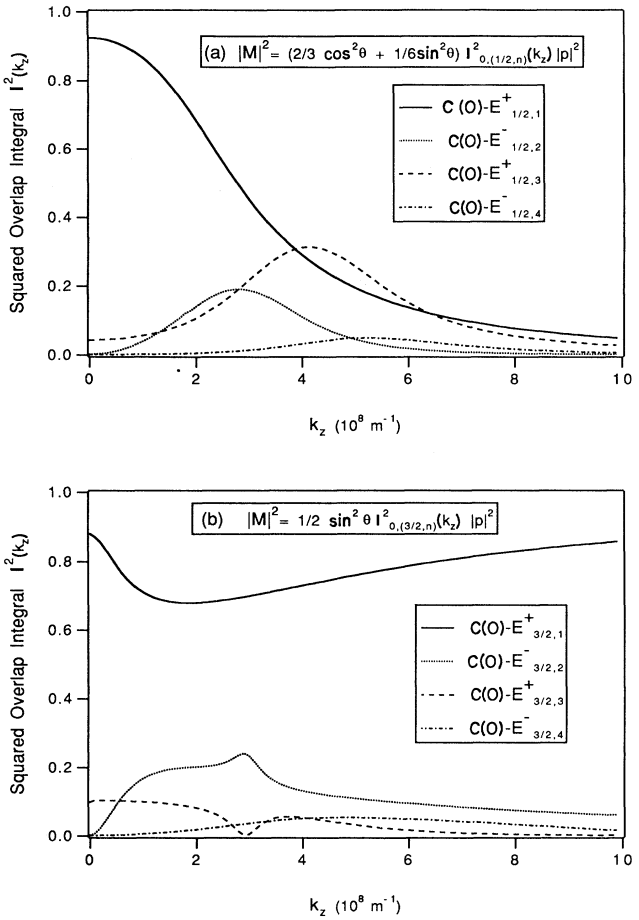

FIG. 5. Squared overlap integral for transitions between $C(0)$ and valence subbands with quantum number (a) $F_z=\pm\frac{1}{2}$ and (b) $F_z=\pm\frac{3}{2}$. The calculation is performed for a 5-nm-radius GaAs quantum wire embedded in an $Al_{0.3}Ga_{0.7}As$ barrier.

Continuing in this fashion, we can derive expressions for the matrix element for transitions involving higher conduction subbands. For a 5-nm-radius GaAs quantum wire embedded in $Al_{0.3}Ga_{0.7}As$, there is only one other bound conduction subband, $C(1)$, which corresponds to quantum number $L_z=\pm1$. This subband is actually fourfold degenerate due to the additional twofold spin degeneracy. Application of the calculational procedure just developed leads to the following results:

$$|M|^2_{C(1)-E_{1/2,n}}=\tfrac{1}{2}\sin^2(\theta)|P|^2 I^2_{-1,(1/2,n)}(k_z)+[\tfrac{2}{3}\cos^2(\theta)|P|^2+\tfrac{1}{6}\sin^2(\theta)|P|^2]I^2_{1,(1/2,n)}(k_z)\ , \tag{14}$$

$$|M|^2_{C(1)-E_{3/2,n}}=[\tfrac{2}{3}\cos^2(\theta)|P|^2+\tfrac{1}{6}\sin^2(\theta)|P|^2]I^2_{1,(3/2,n)}(k_z)\ , \tag{15}$$

Note that, in contrast to the transitions involving the ground conduction subband, the polarization dependence in Eq. (14) involves the overlap integrals, and thus depends upon the radius and composition of the wire, as well as on k_z. The overlap integrals in these equations are defined as follows: $I_{-1,(1/2,n)}$ is the radial overlap between the first excited conduction state $C(1)$ and the component $f_n^3(r)$ of valence state $E_{1/2,n}$; $I_{1,(1/2,n)}$ is the radial overlap of $C(1)$ and the component $f_n^3(r)$ of valence state $E_{1/2,n}$; and $I_{1,(3/2,n)}$ is the radial overlap between $C(1)$ and the component $f_n^2(r)$ of valence state $E_{3/2,n}$. In Figs. 6(a) and 6(b), we plot the squared transition matrix element for transitions involving the $F_z=\frac{1}{2}$ valence states and $C(1)$ for electric fields oriented parallel and perpendicular to a 5-nm-radius GaAs quantum wire embedded in $Al_{0.3}Ga_{0.7}As$ as a function of down-wire momentum, k_z. Figure 7 shows the k_z dependence of the matrix element connecting $C(1)$ of the various $F_z=\frac{3}{2}$

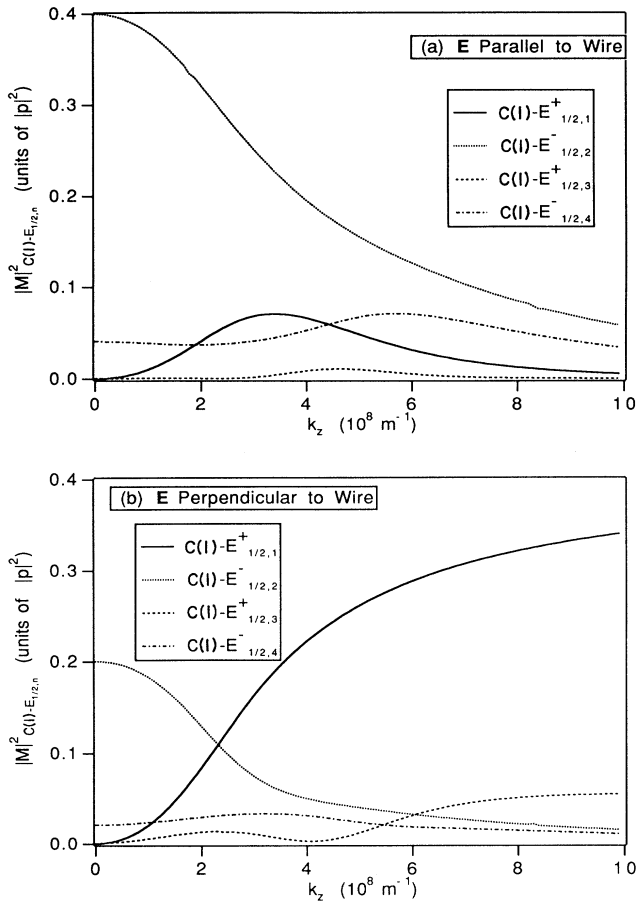

FIG. 6. Squared optical matrix elements for the transitions between $C(1)$ and valence subbands with quantum number $F_z=\pm\frac{1}{2}$. (a) Electric field oriented parallel to the wire; (b) Electric field oriented perpendicular to the wire. The calculation is performed for 5-nm-radius GaAs quantum wire embedded in an $Al_{0.3}Ga_{0.7}As$ barrier. The curves are plotted in units of $|P|^2$ vs down-wire momentum k_2.

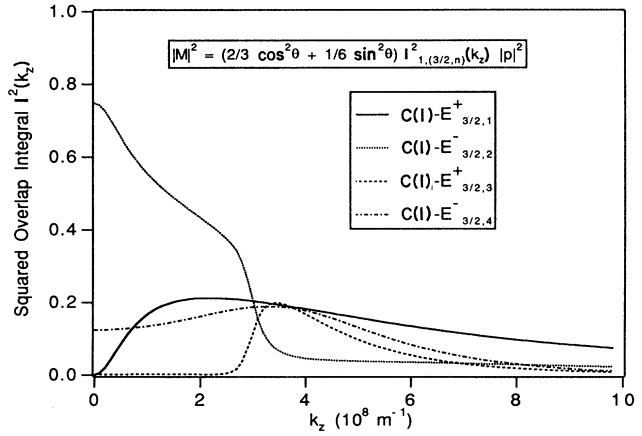

FIG. 7. Squared overlap integral for transitions between $C(1)$ and valence subbands with quantum number $F_z=\pm\frac{3}{2}$, plotted vs down-wire momentum k_z. The calculation is performed for a 5-nm-radius quantum wire embedded in an $Al_{0.3}Ga_{0.7}As$ barrier.

states. The polarization dependence for these transitions is the same as that depicted in Fig. 3 for the transitions connecting $C(0)$ conduction subbands to the $F_z=\frac{1}{2}$ valence subbands.

B. Absorption and emission spectra

Figures 4–7 encompass all possible transitions among bound conduction and valence subbands for a 5-nm-radius GaAs quantum wire with an $Al_{0.3}Ga_{0.7}As$ barrier. Now that we have determined the polarization dependence of the optical-transition matrix elements for these transitions, we are in a position to calculate polarization-dependent absorption and emission spectra for the 5-nm-radius wire. To do so requires a knowledge of the joint density of states (JDOS) for interband transitions. This is simplified by the k selection rule in k_z. For such momentum-conserving transitions, the JDOS may be written

$$J(\hbar\omega)=\sum_{c,v}\frac{2}{\pi}\left|\frac{dk_z}{dE_{c,v}}\right|_{E_{c,v}=\hbar\omega}, \tag{16}$$

where c,v symbolizes the conduction and valence subband indices and k_z satisfies $E_{c,v}=E_c(k_z)-E_v(k_z)$. The factor of 2 accounts for the twofold Kramer's degeneracy. In Figs. 8(a) and 8(b) we separately plot the JDOS for

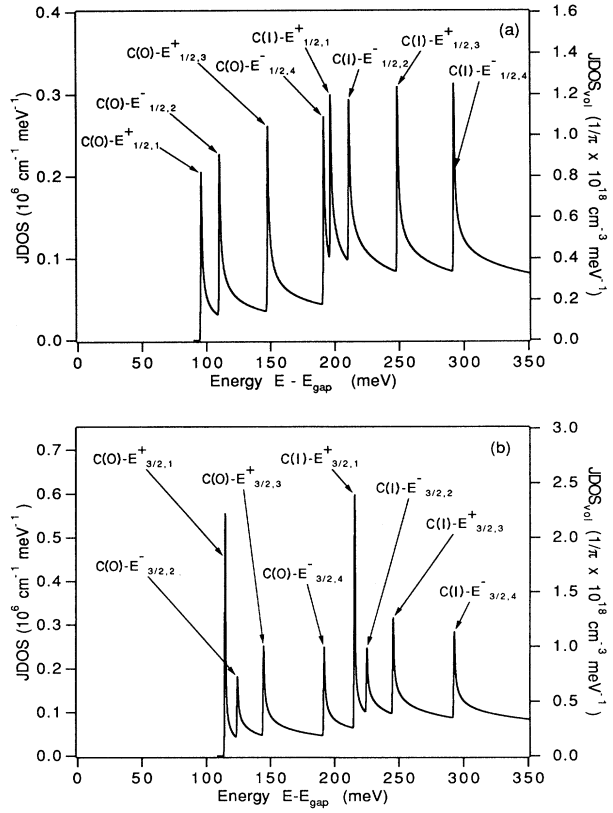

FIG. 8. Joint density of states for a 5-nm-radius GaAs quantum wire embedded in an $Al_{0.3}Ga_{0.7}As$ barrier. (a) JDOS for transitions involving valence subbands with quantum number $F_z=\pm\frac{1}{2}$; (b) JDOS for transitions involving valence subbands with quantum number $F_z=\pm\frac{3}{2}$.

transitions involving the valence subbands corresponding to $F_z=\frac{1}{2}$ and $\frac{3}{2}$, respectively. The curves plotted actually represent a convolution of the JDOS, Eq. (16), with a Gaussian sampling function of width 0.5 meV, so as to smooth out singularities in the JDOS. It is interesting to compare the JDOS at the onset of the lowest-energy transition in Fig. 8(a), denoted $C(0)$-$E^{+}_{1/2,1}$, with that of the lowest transition in Fig. 8(b), $C(0)$-$E^{+}_{3/2,1}$. Due to band repulsion effects, the JDOS for the latter transition is nearly three times larger at its peak than for the lower-energy transition.

With the JDOS and transition matrix elements determined, we can create theoretical polarization-dependent absorption spectra according to the formula

$$\alpha(\hbar\omega)=\frac{\alpha_0}{\omega}\sum_{c,v}\alpha_{c,v}(\hbar\omega)\ . \tag{17}$$

Here, the constant α_0 is given in SI units by

$$\alpha_0=\frac{\pi e^2}{\epsilon_0 c n m_0^2}\ , \tag{18}$$

where n is the refractive index, c is the speed of light in vacuum, ϵ_0 is the permittivity of vacuum, and m_0 is the free-electron mass. The partial absorption $\sum_{c,v}\alpha_{c,v}(\hbar\omega)$ on the transition between conduction and valence states indexed by c,v is given by

$$\alpha_{c,v}(\hbar\omega)=|M|^2_{c,v}\frac{2}{\pi}\frac{1}{\pi R^2}\left|\frac{dk_z}{dE_{c,v}}\right|_{E_{c,v}=\hbar\omega}\ . \tag{19}$$

$|M|^2_{c,v}$ is obtained from Eqs. (12)–(15) and again k_z satisfies $E_{c,v}=E_c(k_z)-E_v(k_z)$. The factor $1/\pi R^2$ gives a volumetric JDOS.

In Figs. 9(a) and 9(b) we show simulated absorption spectra for a 5-nm-radius quantum wire with the same material parameters as above for an electric field oriented parallel and perpendicular to the wire, respectively. The effects of the polarization dependence given in Eqs. (12) and (13) are clear in these figures. There is a large polarization anisotropy between the two lowest-energy transitions, denoted $C(0)$-$E_{1/2,1}$ and $C(0)$-$E_{3/2,1}$ in Figs. 9(a) and 9(b). This relative anisotropy is plotted in Fig. 9(c). We point out that this result is in qualitative agreement with experimental PLE results in which relative anisotropy of the two lowest-energy optical transitions in quantum-wire arrays was studied as a function of the polarization of incident light relative to the wires.[7,8,13]

We are now close to an answer to the question posed in the Introduction concerning the optimal geometry for a quantum-wire laser. Given that the lowest-energy transition in Fig. 9 is strongest when the electric field is parallel to the quantum wire, the optimal geometry of a quantum-wire laser corresponds to Fig. 1(a), where the wires are fabricated parallel to the end facets of the laser (assuming that the laser is operating in TE mode). However, due to the strength of the next-highest energy transition, this conclusion may be modified if the energy splitting between these two lines is small with respect to kT. For example, in a quantum wire of radius 10 nm, the spacing between these transitions is only 5 meV. The optimal configuration for a quantum-wire laser incorporating such relatively large quantum wires might therefore actually be represented by Fig. 1(b), in which the wires are parallel to the optical axis.

Examination of the effect of wire size on the emission

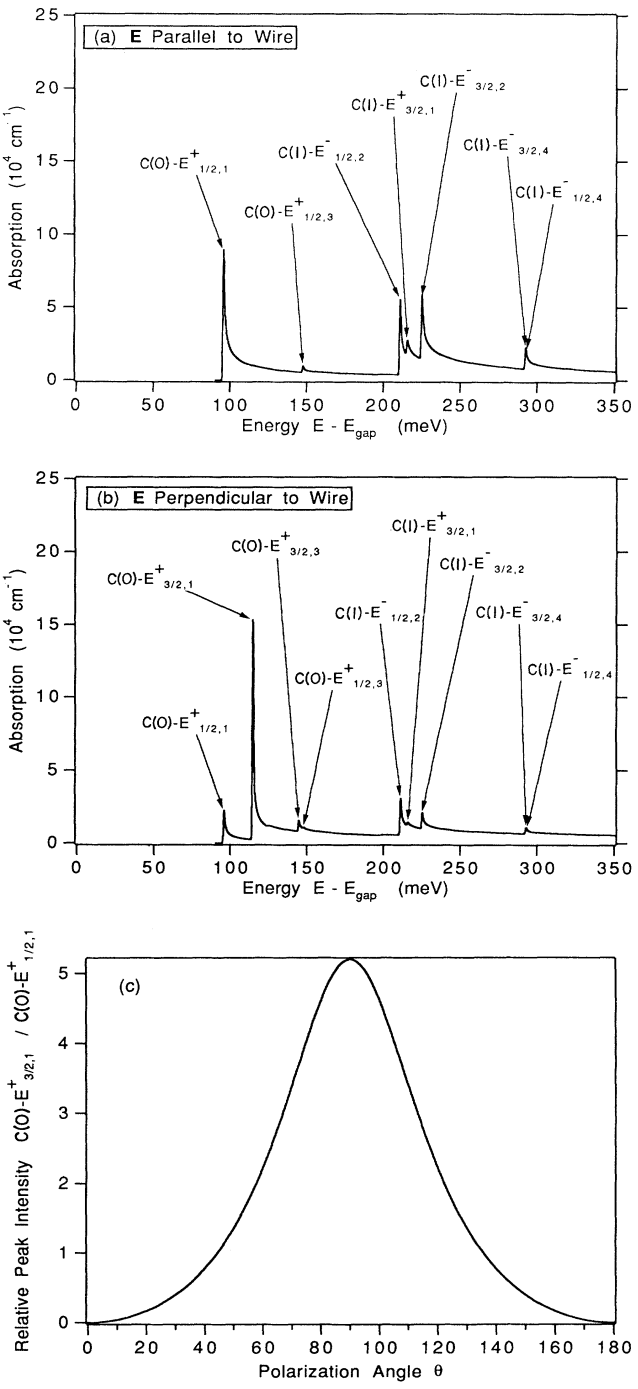

FIG. 9. Simulated absorption spectra for a 5-nm-radius GaAs quantum wire embedded in an $Al_{0.3}Ga_{0.7}As$ barrier. (a) Electric field polarized parallel to the quantum wire; (b) Electric field polarized perpendicular to the wire; (c) Relative polarization dependence of the two peaks labeled "$C(0)$-$E^{+}_{1/2,1}$" and "$C(0)$-$E^{+}_{3/2,1}$" in (a) and (b).

spectra serves to illustrate this point. The emission spectrum is

$$\varepsilon(\hbar\omega)=\frac{\alpha_0}{\omega}\frac{c}{n}\hbar\omega\rho(\hbar\omega)\sum_{c,v}\varepsilon_{c,v}(\hbar\omega)\ , \tag{20}$$

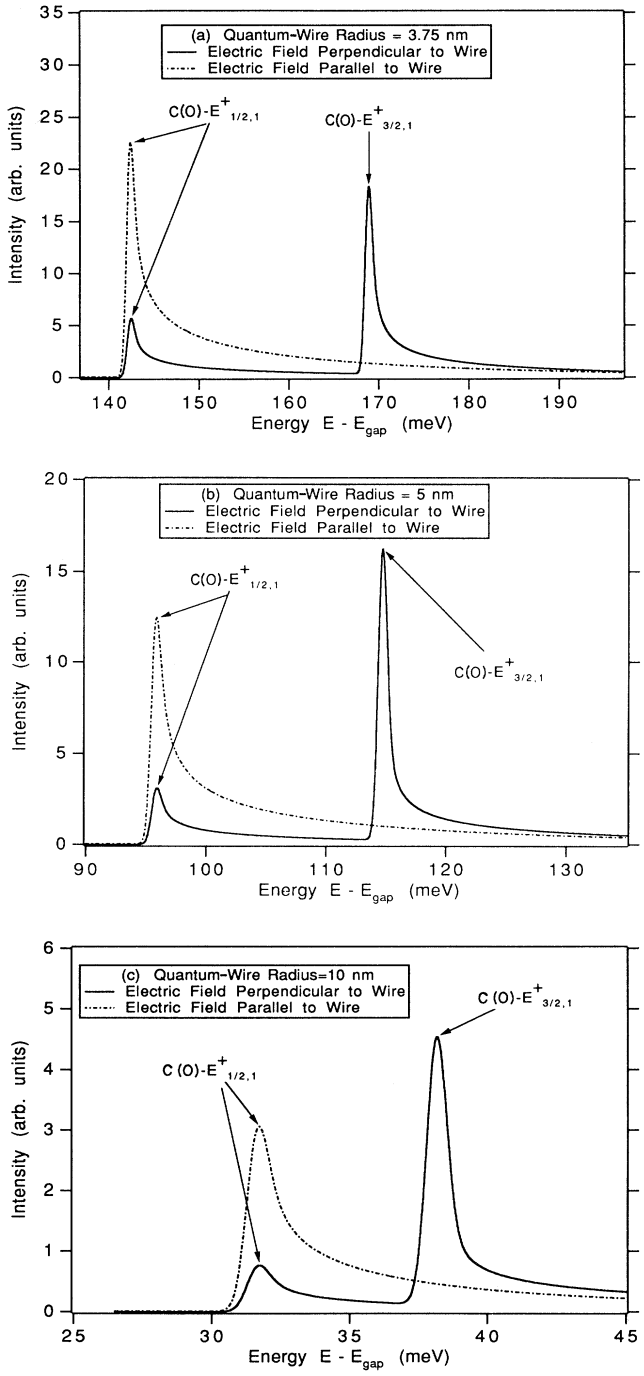

FIG. 10. Simulated room-temperature emission spectra for the GaAs quantum wire embedded in an $Al_{0.3}Ga_{0.7}As$ barrier. (a) Quantum wire radius $=3.75$ nm; (b) quantum wire radius $=5$ nm; (c) quantum wire radius $=10$ nm. In each figure, the solid line corresponds to an electric field polarized perpendicular to the quantum wire, and the dashed line corresponds to an electric field polarized parallel to the wire.

where the optical mode density $\rho(\hbar\omega)$ is

$$\rho(\hbar\omega)=\frac{(\hbar\omega)^2 n^3}{\pi^2\hbar^3 c^3} \tag{21}$$

and the partial emission $\varepsilon_{c,v}(\hbar\omega)$ on the transition between conduction and valence states indexed by c,v is given by

$$\varepsilon_{c,v}(\hbar\omega)=|M|^2_{c,v}\frac{1}{\pi R^2}\frac{2}{\pi}\left|\frac{dk_z}{dE_{c,v}}\right|_{E_{c,v}=\hbar\omega} \times f_C[E_c(k_z)]\{1-f_v[E_v(k_z)]\}\ . \tag{22}$$

Here, $|M|^2_{c,v}$ is obtained from Eqs. (12) and (13) and k_z satisfies $E_{c,v}=E_c(k_z)-E_v(k_z)$. The f_C and f_V are quasi-Fermi-levels for the conduction and valence bands. In Figs. 10(a)–10(c) we show calculated polarization-resolved, room-temperature emission spectra for GaAs quantum wires of radii 3.75, 5, and 10 nm, respectively, embedded in $Al_{0.3}Ga_{0.7}As$. In each case, the Fermi levels for the conduction and valence bands are located just at the position of the lowest-energy electron and hole states, $C(0)$ and $E^+_{1/2,1}$, respectively. In the 3.75-nm-radius quantum wire, the energy splitting between the two lowest-energy lines is 25 meV. As a result, emission is predominantly polarized parallel to the wires. In Figs. 10(b) and 10(c) the energy separation between the two lines is successively reduced and the emission is increasingly polarized transverse to the quantum wires, due to the large density of states of the $F_z=\frac{3}{2}$ valence subband, $E^+_{3/2,1}$. This effect is clearest in Fig. 10(c), in which the line spacing is only 5 meV.

IV. QUANTUM WIRES OF LOWER SYMMETRY

Our discussion of the subband dispersion, DOS, and interband optical-transition matrix elements has been vastly simplified due to the high symmetry of the cylindrical model we have chosen for the quantum wire. The primary reason for choosing such a symmetrical geometry is simply that the problem becomes extremely complex when lower-symmetry structures are considered. However, it is possible using the theory of groups to make certain judgments regarding the polarization dependence of optical transitions in structures of lower symmetry, in particular quantum wires of a square, triangular, and rectangular cross section (Fig. 11). This is valuable since several promising fabrication technologies produce wires of these shapes. The techniques include growth of vertical superlattices on vicinal substrates[7,8] and lateral confinement by strain modulation,[13] both of which result in quantum wires of square or rectangular symmetry, and growth of wires with an equilateral triangular cross section by selective organometallic vapor phase epitaxy.[20]

In order to apply group arguments, we must characterize the symmetry of the states in these lower-symmetry structures. If we imagine adiabatically deforming a cylindrical quantum wire into the shape of a square, triangular, or rectangular wire, it is reasonable to assume that the lowest-lying states will adjust themselves adiabatically to the new geometries. If the cross-sectional area

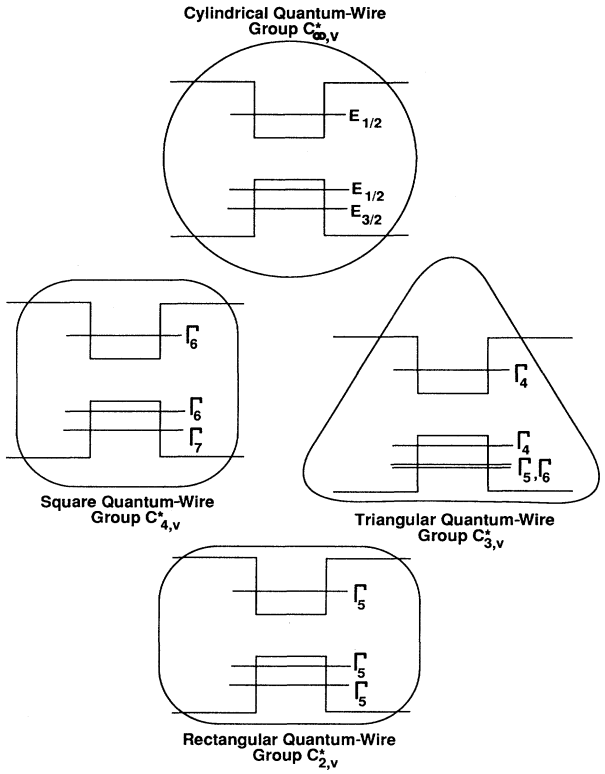

FIG. 11. Schematic representation of the effect of imposing (a) square, (b) rectangular, and (c) triangular symmetry upon a cylindrical quantum wire. The states are labeled for the cylinder according to the irreducible representations of the group $C^*_{\infty,v}$ to which they correspond. The resulting symmetry of the states in (a)–(c) are labeled following the notation of Ref. 21.

remains constant, the subbands will not shift too dramatically, but degeneracies may be lifted. In this case, we can determine the new symmetries and degeneracies by decomposing the appropriate irreducible representations of $C^*_{\infty,v}$ into those of the groups $C^*_{4,v}$, $C^*_{3,v}$, and $C^*_{2,v}$, which describe the square, triangular, and rectangular quantum wire, respectively. This is shown schematically in Fig. 11. Having identified the symmetries of the lowest-energy conduction and valence subbands in the lower-symmetry quantum wires, it is simple to develop matrix element selection rules. As in the cylinder, in each case the component of the dipole operator along the z axis transforms as the identical representation. Thus, transitions between the lowest-lying conduction subband and the second highest valence subband cannot proceed through optical waves polarized along the z axis in the case of the cylindrical, square, or triangular quantum wires. On the other hand, interactions through optical waves polarized perpendicular to the wire are allowed. Hence, Fig. 9(c), which shows relative polarization anisotropy of the two lowest-energy optical transitions in the cylindrical quantum wire, will qualitatively describe the polarization anisotropy of the two lowest-energy transitions in the square and triangular quantum wires. In the case of the rectangular quantum wire, all components of the dipole operator give rise to allowed transitions. The physical basis of this loss of our selection rule for z-polarized light is that a perturbation of rectangular symmetry causes mixing between $F_z=\frac{1}{2}$ and $\frac{3}{2}$ valence subbands of the cylinder. The validity of this interpretation is borne out by the analysis of the valence-subband structure of rectangular quantum wires found in Ref. 18.

V. CONCLUSIONS

We have presented an analytical study of the subband structure, density of states, interband optical-transition matrix elements, and optical-absorption and emission spectra in cylindrical GaAs quantum wires. Band-coupling effects have been shown to be critical to a correct analysis of these properties. We have derived simple trigonometric expressions for the polarization dependence of the optical-transition matrix elements. Additionally, the effects of subband repulsion due to the no-crossing rule of coupled states leads to singularities in the valence-subband DOS. For small quantum wires in which the energy separation between the two lowest valence subbands is larger than kT, the wires should be oriented parallel to the cavity mirrors. This orientation maximizes the transition matrix element for the $C(0)$-$E^+_{1/2,1}$ transition by forcing the electric field to be parallel to the wires. On the other hand, for weakly confined quantum wires in which this energy separation is less than kT, the wires can be oriented parallel to the optical axis of the laser so as to maximize the transition strength between $C(0)$ and the $E^+_{3/2,1}$ valence subband, which has the largest DOS. We showed by application of group theory that these general conclusions remain qualitatively valid in quantum wires of lower symmetry, such as wires with a square, rectangular, and triangular cross section.

ACKNOWLEDGMENTS

This work was supported by grants from the National Science Foundation and the Office of Naval Research. P.S. gratefully acknowledges support received from the National Science Foundation.

[1]Yasuhiko Arakawa, Kerry Vahala, and Amnon Yariv, Appl. Phys. Lett. **45**, 950, (1984).
[2]Hal Zarem, Kerry J. Vahala, and Amnon Yariv, IEEE J. Quantum Electron. **25**, 705 (1989).
[3]Kerry J. Vahala, IEEE J. Quantum Electron. **24**, 523 (1988).
[4]E. Kapon, D. M. Hwang, and R. Bhat, Phys. Rev. Lett. **63**, 430 (1989); see also E. Kapon, S. Simhony, R. Bhat, and D. M. Huang, Appl. Phys. Lett. **55**, 2715 (1989).
[5]Masahiro Asada, Yasuyuki Miyamoto, and Yasuharu Suematsu, Jpn. J. Appl. Phys. **24**, L95, (1985).
[6]Masahiro Asada, Yasuyuki Miyamoto, and Yasuharu Suematsu, IEEE J. Quantum Electron. **9**, 1915 (1986).

[7]M. Tsuchiya, J. M. Gaines, R. H. Yan, R. J. Simes, P. O. Holtz, L. A. Coldren, and P. M. Petroff, Phys. Rev. Lett. **62**, 466 (1989).
[8]Masaaki Tanaka and Hiroyuki Sakaki, Appl. Phys. Lett. **54**, 1326 (1989).
[9]Peter C. Sercel and Kerry J. Vahala, in *The International Quantum Electronics Conference, 1990, Technical Digest Series* (Optical Society of America, Washington, DC, 1990), Vol. 8, pp. 204 and 205.
[10]Kerry J. Vahala and Peter C. Sercel, Phys. Rev. Lett. **65**, 239 (1990).
[11]Peter C. Sercel and Kerry J. Vahala, Phys. Rev. B **42**, 3690 (1990).
[12]Peter C. Sercel and Kerry J. Vahala, Appl. Phys. Lett. **57**, 545 (1990).
[13]D. Gershoni, J. S. Weiner, S. N. G. Chu, G. A. Baraff, J. M. Vandenberg, L.N. Pfeiffer, K. West, R. A. Logan, and T. Yanbun-Ek. Phys. Rev. Lett. **65**, 1631 (1990).
[14]Mark Sweeny, Jingming Xu, and Michael Shur, Superlatt. Microstruct. **4**, 623 (1988).
[15]J. M. Luttinger and W. Kohn, Phys. Rev. **97**, 869 (1955).
[16]J. M. Luttinger, Phys. Rev. **102**, 1030 (1956).
[17]J. A. Brum, G. Bastard, L. L. Chang, and L. Esaki, Superlatt. Microstruct. **3**, 47 (1987).
[18]D. S. Citrin and Yia-Chung, Phys. Rev. B **40**, 5507 (1989).
[19]Evan O. Kane, J. Phys. Chem. Solids **1**, 249 (1957).
[20]John A. Lebens, Charles Tsai, Kerry J. Vahala, and Thomas Kuech, Appl. Phys. Lett. **56**, 2642 (1990).
[21]George F. Koster, John O. Dimmock, Robert G. Wheeler, and Hermann Statz, *Properties of the Thirty-Two Point Groups* (MIT Press, Cambridge, 1963).